Optical-luminescence properties of ZnO and TiO$_2$ nanopowders obtained by pulsed laser reactive ablation

Yu. I. Venhryn[1], I. D. Popovych[3], A. S. Serednytski[1,*] (iD), O. F. Kolomys[2], A. P. Luchechko[3], and V. V. Strelchuk[2]

[1] *Pidstryhach Institute for Applied Problems of Mechanics and Mathematics NASU, Naukova Str., 3b, Lviv 79060, Ukraine*

[2] *Lashkaryov Institute of Semiconductor Physics of the NAS of Ukraine, Kyiv, Ukraine*

[3] *Electronics and Computer Technologies Department, Ivan Franko National University of Lviv, 50 Dragomanov Street, Lviv 79005, Ukraine*

ABSTRACT

The ZnO and TiO$_2$ nanopowders have been prepared by means of the pulsed laser reactive ablation of metallic (Zn, Ti) targets. The Structural, optical, and luminescent studies have been done using by X-ray diffractometry, electron microscopy, transmission, Raman and photoluminescent spectroscopy. All nanopowders having high optical transmission in the visible and near-IR regions of the spectrum. Based on the phonon mode analysis in the Raman spectrum of nanopowders the character of the quality of the crystal structure are determined and its evolution in the process of laser annealing. It was found that pulsed laser annealing makes it possible to significantly modify the luminescent properties of nanopowders by changing its intrinsic defective structure. Dependence of the photoluminescence intensity on excitation wavelength have been studied and the optimal wavelengths to excitation the luminescence were established.

1 Introduction

Nanopowder (NP) metal oxides ZnO and TiO$_2$ are promising wide-band, non-toxic semiconductor materials that are widely used in various practical fields and attract considerable attention of researchers due to the possibility of creating on their basis a various of devices [1–3], including gas sensors [4–7]. It is known that the processes of gas adsorption are associated with electronic transitions on the surface of the material, and this leads to various effects in luminescence [8, 9] and these processes are particularly pronounced in NP materials with a large effective surface [4]. Moreover the properties of the nanomaterial can be further modified by laser annealing [7] surface doping [10] or prepare composite from a few NPs [11].

A number of methods of nanopowder fabrication are known include the ablation in liquid [12]. Each

---

method has advantages and disadvantages. Liquid phase methods are cost-effective and are used for synthesizing various kinds of nanoparticles with well-controlled structures at the laboratory scale. Vapor phase processes are superior at synthesizing high purity nanoparticles by means of the continuous flow reactor [13]. Also, materials with core–shell morphology and heterojunction structure cannot be produced by ablation in liquid [14], which could be important in gas sensor field [15]. Other laser fabrication method synthesis using CO_2-laser during evaporation of metal oxide targets [16]. However, in this method there is no dosed control of pressure and composition of reactive gas which fact does not enable to form composite nanopowder materials and barrier structures on their basis during evaporation of metal targets. Besides, for evaporation of mainly transparent targets of metal oxides it is necessary to use CO_2—or eximer lasers, this fact limiting the use of accessible and low-price solid-state powerful lasers which work in visible or near infrared spectral regions for that purpose. Another promising method for obtaining a wide class of NP materials is pulsed laser reactive technology [17–19]. This method allows to regulate the technological parameters of the process and, accordingly, the characteristics of the synthesized NPs. The formation of the dispersed phase takes place under conditions of high growth rates and process rates, which leads to the formation of a nonequilibrium structure of the material ZnO and TiO_2, which have pronounced self-defective structure [18].

The work is devoted to the study of optical and luminescent characteristics of NPs of zinc and titanium oxides obtained by the optimized method of laser ablation of metal targets in a chemically active environment and the effect of laser annealing on its properties. Established the role defects of crystal lattice in the formation of luminescence centers and excitation energy transfer processes. The obtained results are important, particular, can help increasing the selectivity of the gas-sensitive materials and accordingly, gas sensors in general.

2 Experimental

The metal oxide NPs were obtained by optimizing the processes of pulsed laser evaporation of metal targets (Zn, Ti) by means of a YAG: Nd^{3+} laser

($\lambda = 1.06$ μm, $\tau = 10^{-7}–10^{-5}$ s, $q = 10^6 \div 10^7$ W/cm^2, $n = 14–56$ Hz, $d = 5$ mm, $E_i = 0.005–0.350$ J) in a directional flow of a mixture of reactive (O_2) and inert (He, Ar) gases in a given proportion, at atmospheric pressure. The flow of the gas mixture was directed parallel to the target by means of the fan with the set speed [20], which provided transfer and separation of powder with its subsequent collection at an exit from the reaction chamber by means of a special cyclone and filters. By regulating the partial pressure of the reactive gas, full or partial (near-surface) oxidation of the NP is provided.

Laser annealing of NPs was carried out in the range of material transparency using a YAG: Nd^{3+} laser ($\lambda = 1.06$ μm, $\tau = 10^{-8}–10^{-3}$ s, $q = 10^5 \div 10^8$ W/cm^2, $n = 14–56$ Hz, $d = 5$ mm, $E_i = 0.005–0.350$ J). The laser radiation was focused, using a lens, on a NPs, housed in a quartz cuvette placed on a specially designed vibrating device with an oscillation frequency in the range of 10–60 Hz. Due to such vibrational oscillations, the NP was well mixed, which allowed to obtain a uniform annealing of the entire volume of particles.

Phase and structural analyses of nanopowders were performed using electron microscopes: scanning Carl Zeiss EVO 40XVP with an OXFORD INCA Energy 350 energy dispersive annex and transmission a SELMI PEM-125K with an operating voltage up to 100 kV. Diffraction patterns have been obtained with using of powder diffractometer with special high temperature attachment was obtained with help of graphite single crystal, installed in diffraction beam. Experimental data were recorded and analyzed with help of software package DHN-PDS that allowed us to determine the diffraction angles, half-height width, and values of cell parameters with high accuracy. Size of nanoparticles was estimated with help of Scherrer formula: $L = \lambda/[\beta \cdot \cos(\theta)]$, where β-half-height width of reflex.

Raman scattering (RS) spectra were excited by Ar^+/Kr^+ laser with a wavelength of 514.5 nm and recorded at room temperature in the backscattering geometry using a triple spectrometer Horiba Jobin–Yvon T-64000 equipped with an Olymp BX41 confocal focusing microscope (to focus the radiation a $50 \times$ lens with a quantitative aperture of 0.8 was used). The laser beam was focused on a spot with a diameter of less than 1 μm and the power of the beam varied within $0.25 \div 25$ mW. The accuracy of

determining the frequency position of the phonon line was not more than 0.2 cm^{-1}.

Studies of the excitation and PL spectra were performed using a Solar CM2203 spectrofluorometer at room temperature. The device provides high accuracy of measurements in the ultraviolet and visible parts of the spectrum (220 ÷ 800 nm), as well as performs automatic correction of excitation and luminescence spectra. For spectral separation of light beams, this device is equipped with diffraction gratings that provide separation up to 0.1 nm. Luminescence was recorded using a Hamamatsu R928 photomultiplier. The source of excitation was a xenon lamp with a power of 150 watts. Diffuse reflection spectra were studied on a Shimadzu UV-3600i Plus spectrophotometer.

3 Results and discussion

Figure 1 shows a typical surface morphology of the obtained ZnO samples. X-ray diffraction patterns of the initial ZnO and TiO$_2$ nanopowders are presented in Fig. 2. The diffraction patterns ZnO (Fig. 2a) have peaks characteristic of the hexagonal wurtzite structure, indexed as planes (100), (002), (101), (102), (110), and (103) ZnO. Peaks corresponding to other oxides or compounds were not detected. The diameter of the obtained nanoparticles is in the range of 40–60 nm as obtained by Scherrer equation. The peaks of the chemical elements Zn and O were detected in the energy dispersion spectroscopy spectra of ZnO nanopowders. Peaks that may correspond to impurities were not detected, which indicates the high purity of the obtained materials. X-ray diffraction
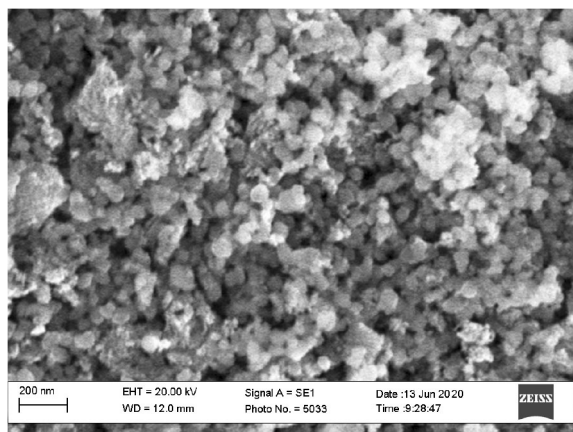

Fig. 1 SEM morphologies of ZnO nanopowders

studies showed that TiO$_2$ samples have a crystalline structure of rutile which is indicated by the peaks corresponding to (110), (101), (111), (211), and (002) plane. The crystallite size was about 60 nm. In the EDS spectra there are peaks of the elements Ti and O, peaks that may correspond to impurities are not detected, this indicates that the obtained materials are pure.

RS spectroscopy is an important tool for studying the structural quality of nanomaterials, their local structure, disorder, and defects. In the RS spectra (Fig. 3a) of the original and laser annealed ZnO powders there are present, allowed by the selection rules, intense E$_2$ (low) and E$_2$ (high) phonon bands at ~ 99 cm^{-1} (G ~ 1.6 cm^{-1}) and ~ 438 cm^{-1} (G ~ 5.0 cm^{-1}), respectively [21]. As is known, E = (low) and E$_2$ (high) correspond to the oscillations of heavy zinc atoms and light oxygen atoms in the cationic and anionic sublattices of wurtzite ZnO in the plane perpendicular to the c axis and, accordingly, are sensitive to the disorder of the crystal structure of ZnO. This is manifested in the Raman spectra of laser annealed ZnO NPs in the broadening and nonmonotonic shift of the maximum E$_2$ (high) band compared to the frequency of bulk ZnO (ω_0 = 437 cm^{-1} [22]), (Fig. 3a, insert), which indicates the heterogeneity of spatial distribution of deformations, structural perfection, and sizes of ZnO nanocrystals. The bands at 380.3 cm^{-1} and 411.8 cm^{-1} are assigned to the transverse-optical A$_1$ (TO) and E$_1$ (TO) modes, respectively. Other bands, located at 203 and 333 cm^{-1} are believed to be second-order Raman scattering that arose from zone-boundary (M point) phonons 2TA (M) or 2E$_2$ (low) and E$_2$ (high)-E$_2$ (Low) (M), respectively. Laser annealing leads to a decrease in the intensity and increase in the half-width of the E$_2$ (Low) and E$_2$ (high) bands, which indicates a disorder of the crystal structure of the material in both zinc and oxygen sublattices. In addition, in the Raman spectra of ZnO nanopowders there is an additional broad band with a complex structure. The intensity of the marked band increases with increased duration of laser annealing. In previous research, an additional broad band at 500–600 cm^{-1} was commonly observed in doped or ion-implanted ZnO samples [23, 24], and was assigned as a defect-related Raman band induced by oxygen vacancy and lattice deterioration due to impurity doping. Its decomposition into elementary Gaussian contours (Fig. 1a, insert) allowed
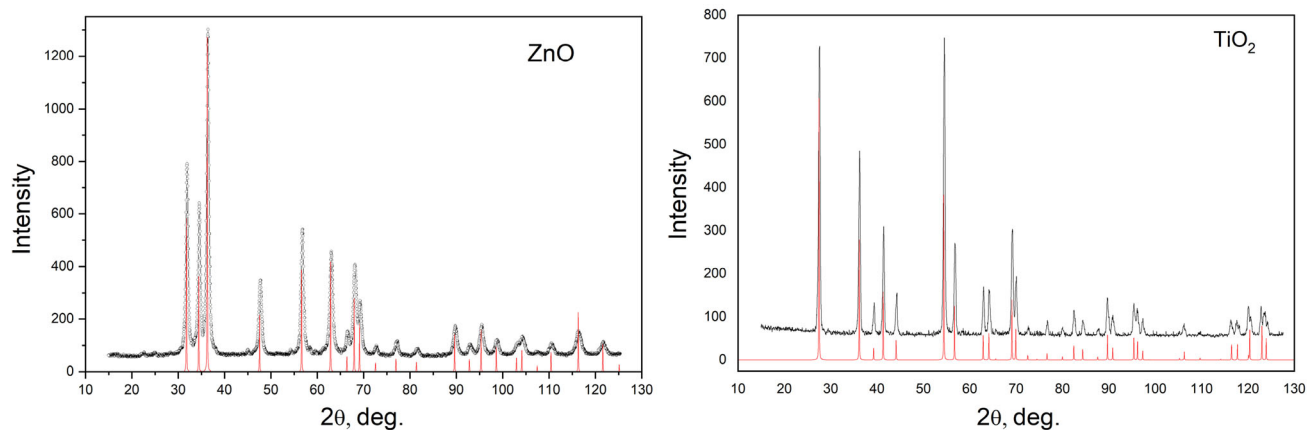
Fig. 2 Diffraction patterns for initial TiO_2 and ZnO nanopowders
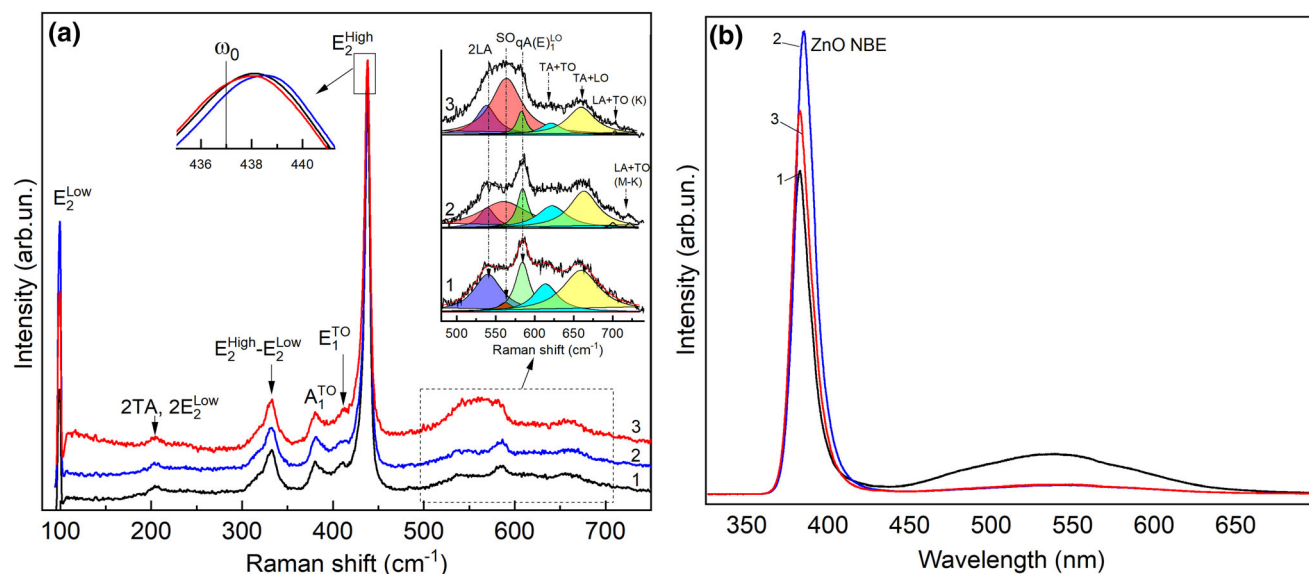

Fig. 3 Raman scattering spectra initial (1) and laser ($\tau = 10$ ns, $n = 28$ Hz, $E = 0.1$ J/cm^2) annealed during 40 min (2), 20 min (3) ZnO nanopowders (**a**) and TiO_2 nanopowders (**b**) initial (1) and annealed 10 min (2), 20 min (3), 40 min (4)

to obtain bands at 539, 618, 660, 664, 700, and 720 cm^{-1} that correspond to the processes of multiphonon scattering by 2LA or 2B$_1$ (Low) (Γ, M), TA + LO (H, M), TA + LO (L, H), TA + LO (M), LA + TO (M), and LA + TO (LM) phonons, respectively [25]. The small intensity of a band at 580 cm^{-1}, the position of which is the superposition of the two A$_1$ (LO) and E$_1$ (LO) modes, is characteristic of the Raman spectra of wurtzite ZnO films due to the process of destructive interference between the Fröhlich interaction mechanism and the strain potential in the scattering process on LO phonons of ZnO [26]. It should be noted, the increase in the contribution of the 562 cm^{-1} band due to increased duration of laser annealing. The nature of this band is

still a debatable one. According to [27], the band at 560 cm^{-1} may be due to surface optical modes (SO) of phonons formed from phonons of A$_1$ or E$_1$ symmetry. Therefore, the increase in its intensity may be associated with an increase in the ratio of the surface to the volume of ZnO nanocrystals.

Raman spectra (Fig. 3b) of the original and laser annealed TiO_2 samples are typical for the crystalline phase of rutile [28]. In the spectra there are intense modes with a frequency position of 145 cm^{-1} (B$_{1G}$), 446 cm^{-1} (E$_G$), 610 cm^{-1} (A$_{1G}$). The broad band at 241 cm^{-1} has been attributed to second-order or two-phonon Raman scattering, and so cannot be counted among the four fundamental modes predicted by group theory. Laser treatment leads to an increase in

the intensity and reduction of the half-width of the bands of all modes, peaks of all modes, which may be due to the improvement of the structural ordering of TiO_2 within the volume.

Obtained nanopowders have high optical transmission in the visible and near-IR regions of the spectrum (Fig. 4). TiO_2 NPs have a high optical transmittance in the visible and near-IR regions of the spectrum.

Figure 5a shows the PL spectra of the initial and laser annealed ZnO NPs. It was found that an intense ultraviolet peak (385 nm) and a wide yellow–green band (~ 540 nm) were observed in the PL spectra for all ZnO samples at room temperature. This nature of the PL luminescence proves the high structural perfection of the ZnO NPs formed by us using the optimized laser reactive technology. The observed yellow-green luminescence band of NP ZnO may be due to oxygen defects, in particular, excess oxygen [29]. This band is clearly non-elementary, probably due to the presence of similar centers of luminescence. Negatively charged zinc vacancy can be localized near certain positively charged defects of the ZnO crystal lattice, forming several luminescence centers of different composition. The shift of the luminescence band of NP ZnO after laser annealing is obviously the result of the redistribution of the intensities of the elementary bands that make up the complex yellow–green band.
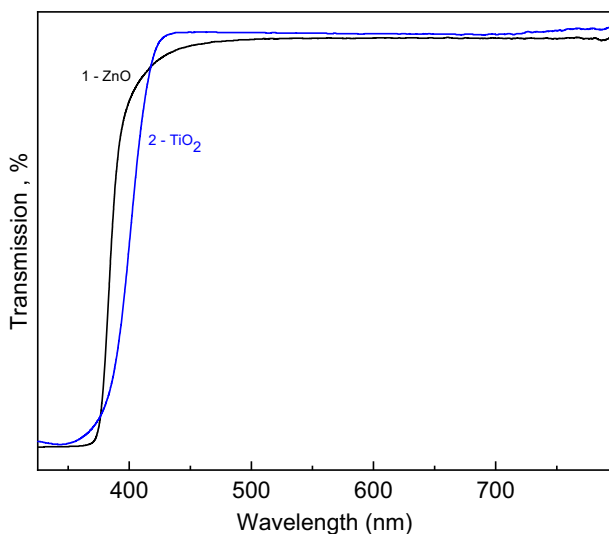
For NPs TiO_2 there is a wide band of photoluminescence in the visible region (400–650 nm) (Fig. 5b). The decomposition of the photoluminescence spectrum of the TiO_2 nanopowder (laser annealing during 40 min) into elementary components by Gaussian contours is presented in insert Fig. 5b. The most likely defects responsible for the visible band of the PL are oxygen vacancies [30]. A neutral oxygen vacancy is responsible for a peak at 465 nm, a positively charged oxygen vacancy may correspond to a PL band with a maximum at 523 nm. A high-energy wing with a maximum at 585 nm is also associated with the presence of oxygen vacancies on the surface of TiO_2, which are differently filled with electrons [31]. The appearance of these charged centers is due to the fact that TiO_2 is nonstoichiometric in oxygen and in the structure of the crystal, as a rule, there are always oxygen vacancies. One oxygen vacancy leads to the formation of two charged Ti^{3+} centers on the TiO_2 surface. It was found that pulsed laser annealing makes it possible to significantly modify the luminescent properties of NP TiO_2 by changing its intrinsic defective structure.

To study the characteristics of the surface energy states of NP ZnO associated with visible luminescence, studies of changes in the intensity of ultraviolet (387 nm) and green (520 nm) maxima of luminescence depending on the wavelength of excitation were performed (Fig. 6). The nature of the photoluminescence spectrum of NP ZnO practically does not depend on the excitation wavelength in the range $\lambda = 265$–377 nm and indicate the same nature of the luminescence centers. When ZnO NP was excited with energy greater than the band gap, a gradual increase in the luminosity intensity occurred, up to $\lambda_{ex} = 340$ nm for the main ($\lambda_{lum} = 565$ nm) maximum of luminescence (Fig. 3b). The relative intensity of the short-wavelength luminescence maximum at 387 nm increases sharply as the excitation wavelength approaches 365 nm (3.39 eV). This indicates that the efficiency of luminescence excitation is significantly higher near the energy of the band gap and the initial energy states are located slightly below the bottom of the conduction band.

The optimal wavelengths for excitation of visible luminescence, lying in a wide spectral range of 250–385 nm, are established (Fig. 3a). In the excitation spectrum of the green luminescence band ($\lambda_{lum} = 525$ nm) there is a slight decrease in the excitation intensity to $\lambda_{ex} = 375$ nm and the manifestation of a

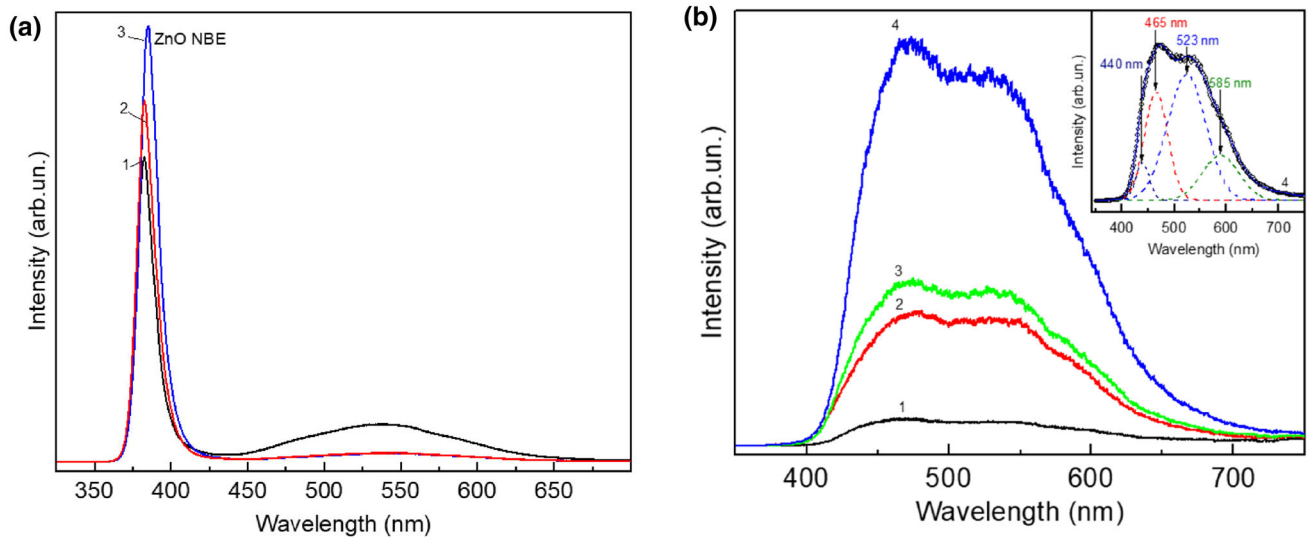**Fig. 4** Optical transmission spectra of initial ZnO (1) and TiO_2 (2) nanopowders

Fig. 5 photoluminescent spectra initial (1) and laser ($\tau = 10$ ns, $n = 28$ Hz, $E = 0.1$ J/cm^2) annealed during 40 min (2), 20 min (3) ZnO nanopowders (**a**) and TiO$_2$ nanopowders (**b**) initial (1) and annealed 10 min (2), 20 min (3), 40 min (4)
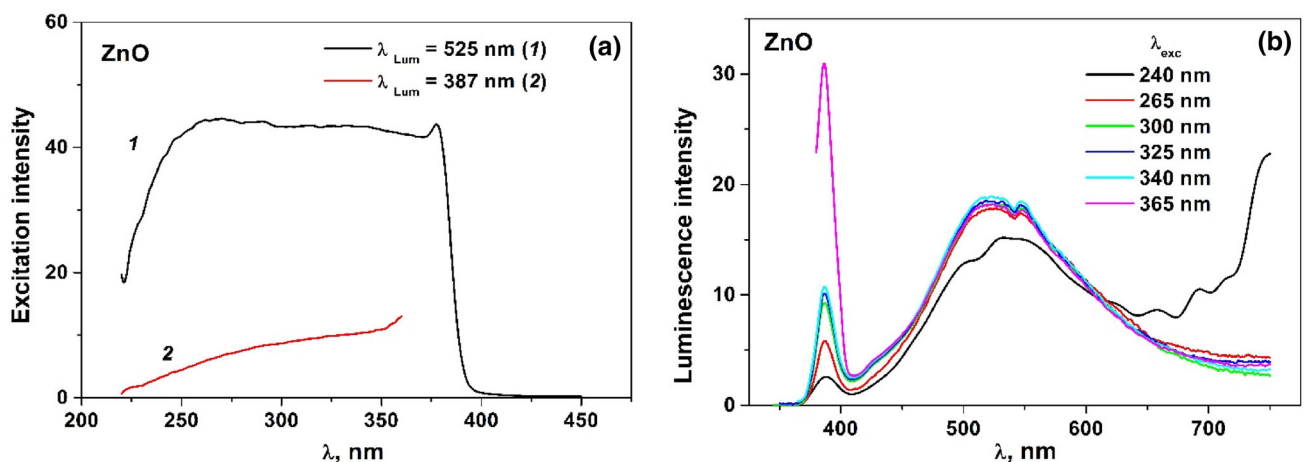

Fig. 6 Excitation (**a**) and photoluminescence (**b**) spectra of ZnO nanopowders

pronounced excitation peak in the vicinity of 380 nm, which obviously corresponds to the exciton excitation energy. Furthermore, there is a sharp decrease in the excitation intensity of this luminescence until its complete quenching at $\lambda_{ex} \geq 400$ nm. For the luminescence maximum at $\lambda_{lum} = 387$ nm with increasing excitation wavelength from 220 to 350 nm, there is a gradual increase in the luminescence intensity with its subsequent sharp increase when approaching the exciton excitation.

The excitation spectrum of photoluminescence of TiO$_2$ NP is characterized by an increase in the luminescence intensity as the excitation wavelength increases in the range of 265–425 nm without a

noticeable change in the nature of the luminescence spectrum itself. However, in the case of NP TiO$_2$, the intensity of luminescence at maxima $\lambda = 440$ and 465 nm with increase of excitation wavelength ($\lambda_{ex} = 265$–380 nm) gradually increases with the subsequent manifestation of luminescence resonances in the region of fundamental absorption of the material (Fig. 7).

4 Conclusion

Peculiarities of photoluminescence of initial and laser annealed ZnO and TiO$_2$ nanopowders prepared by means of the pulsed laser reactive ablation of metallic
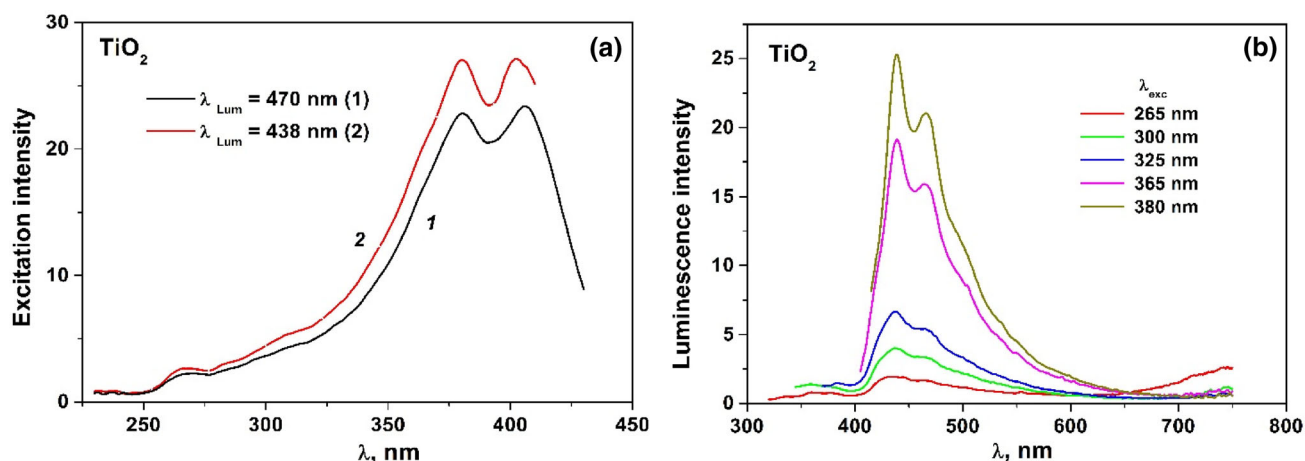
Fig. 7 Excitation (**a**) and photoluminescence (**b**) spectra of TiO_2 nanopowders

target (Zn, Ti) have been studied. The diameter of the obtained nanopowders is in the range of 40–60 nm. Established that pulsed laser annealing makes it possible to significantly modify the luminescent properties of nanopowders by changing its intrinsic defect structure. Based on the phonon mode analysis in the Raman spectrum of nanopowders the character of the quality of the crystal structure are determined and their evolution in the process of laser annealing. The dependence of the photoluminescent intensity of nanopowders on the excitation wavelength has been studied and the optimal wavelengths to excitation the luminescence were established. Changing the excitation wavelength can be effectively used to increase sensitivity of the gas sensor system.

Author contributions

YIV and IDP: experimentation, methodology, and drafting. ASS: experimentation, methodology, original draft preparation, reviewing, and editing of the manuscript. OFK and VVS: Raman and photoluminescent spectroscopy experimentation, writing, and editing. APL: excitation and photoluminescent spectra. All authors have participated in conception and design, analysis, and interpretation of the data, drafting the article or revising.

Data availability

Data sharing is not applicable to this article as only experimental results.

Declarations

Conflict of interest The authors declare that they have no conflict of interest.

References

1. G. Oskam, J. Sol–Gel Sci. Technol. (2006). https://doi.org/10.1007/s10971-005-6621-2
2. Z.L. Wang, J. Phys. Condens. Matter (2004). https://doi.org/10.1088/0953-8984/16/25/R01
3. Y. Wang, Y. He, Q. Lai, M. Fan, J. Environ. Sci. (2014). https://doi.org/10.1016/j.jes.2014.09.023
4. C. Wang, L. Yin, L. Zhang, D. Xiang, R. Gao, Sensors (2010). https://doi.org/10.3390/s100302088
5. Y.F. Sun, S.B. Liu, F.L. Meng, J.Y. Liu, Z. Jin, L.T. Kong, J.H. Liu, Sensors (2012). https://doi.org/10.3390/s120302610
6. V.M. Zhyrovetsky, D.I. Popovych, S.S. Savka, A.S. Serednytski, Nanopowder Nanoscale Res. Lett. (2017). https://doi.org/10.1186/s11671-017-1891-5
7. M. Eltermann, V. Kiisk, A. Berholts, L. Dolgov, S. Lange, K. Utt, R. Jaaniso, Sens. Actuators B Chem. (2018). https://doi.org/10.1016/j.snb.2018.03.034
8. S. Kim, R.M. Dulanga, S. Somaratne, J.E. Whitten, J. Phys. Chem. C (2018). https://doi.org/10.1021/acs.jpcc.8b04715

9. Y.V. Bobitski, R.V. Bovhyra, D.I. Popovych, S.S. Savka, A.S. Serednytski, V.N. Shevchuk, Y.I. Venhryn, J. Nano Electron. Phys. (2017). https://doi.org/10.21272/jnep.9(5).05008

10. V.V. Gafiychuk, B.K. Ostafiychuk, D.I. Popovych, I.D. Popovych, A.S. Serednytski, Appl. Surf. Sci. (2011). https://doi.org/10.1016/j.apsusc.2011.04.084

11. R.V. Bovhyra, S.I. Mudry, D.I. Popovych, S.S. Savka, A.S. Serednytski, Y.I. Venhryn, Appl. Nanosci. (2019). https://doi.org/10.1007/s13204-018-0697-9

12. D. Zhang, Z. Li, K. Sugioka, J. Phys. Photonics **3**, 042002 (2021)

13. Z. Lin, S. Shen, Z. Wang, W. Zhong, iScience (2021). https://doi.org/10.1016/j.isci.2021.102469

14. Z.Y. Douglas, B. Chrisey, J. Photochem. Photobiol. C Photochem. Rev. (2012). https://doi.org/10.1016/j.jphotochemrev.2012.04.004

15. J. Park, J. Kim, A. Min, M.Y. Choi, Environ. Res. (2022). https://doi.org/10.1016/j.envres.2021.112340

16. U. Popp, R. Herbig, G. Michel, E. Müller, C. Oestreich, J. Eur. Ceram. Soc. (1998). https://doi.org/10.1016/s0955-2219(98)00037-5

17. Y.I. Venhryn, S.S. Savka, R.V. Bovhyra, V.M. Zhyrovetsky, A.S. Serednytski, D.I. Popovych, Mater. Today Proc. (2021). https://doi.org/10.1016/j.matpr.2019.11.118

18. B.K. Ostafiychuk, V.M. Zhurovetski, B.K. Kotlyarchuk, M.I. Moysa, D.I. Popovych, A.S. Serednytski, Phys. Chem. Solid State **9**(4), 728–731 (2008)

19. B. Kovalyuk, V. Mocharskyi, Yu. Nikiforov, V. Onisimchuk, D. Popovych, A. Serednytski, V. Zhyrovetsky, Phys. Status Solidi (2013). https://doi.org/10.1002/pssc.201200889

20. I.V. Lazoryk, I.D. Popovych, Yu.I. Venhryn, S.S. Savka, R.V. Bovhyra, A.S. Serednytski, S.I. Mudry, Appl. Nanosci. (2020). https://doi.org/10.1007/s13204-020-01336-8

21. R. Cuscó, E. Alarcón-Lladó, J. Ibáñez et al., Phys. Rev. B. (2007). https://doi.org/10.1103/PhysRevB.75.165202

22. Y.T. Song, X.L. Chen, W.J. Wang et al., J. Cryst. Growth. (2004). https://doi.org/10.1016/j.jcrysgro.2003.08.052

23. T.L. Phan, N.X. Nghia, S.C. Yu, Solid State Commun. (2012). https://doi.org/10.1016/j.ssc.2012.08.026

24. C. Bundesmann, N. Ashkenov, M. Schubert, D. Spemann, T. Butz, E.M. Kaidashev, M. Lorenz, M. Grundmann, Appl. Phys. Lett. (2003). https://doi.org/10.1063/1.1609251

25. R. Cuscó, E. Alarcón-Lladó, J. Ibáñez, L. Artús, J. Jiménez, B. Wang, M. Callahan, Phys. Rev. B (2007). https://doi.org/10.1103/physrevb.75.165202

26. R. Callender, S. Sussman, M. Selders, R. Chang, Phys. Rev. B. (1973). https://doi.org/10.1103/PhysRevB.7.3788

27. A.G. Milekhin, N.A. Yeryukov, L.L. Sveshnikova, T.A. Duda, E.I. Zenkevich, S.S. Kosolobov, A.V. Latyshev, C. Himcinski, N.V. Surovtsev, S.V. Adichtchev, Z.C. Feng, C.C. Wu, D.S. Wuu, D.R.T. Zahn, J. Exp. Theor. Phys (2011). https://doi.org/10.1134/S1063776111140184

28. Y. Zhang, C.X. Harris, P. Wallenmeyer, J. Murowchick, X. Chen, J. Phys. Chem. C (2013). https://doi.org/10.1021/jp406948e

29. Y.W. Heo, D.P. Norton, S.J. Pearton, J. Appl. Phys. (2005). https://doi.org/10.1063/1.2064308

30. Y.-H. Chang, C.-M. Liu, C. Chen, H.-E. Cheng, J. Electrochem. Soc. (2012). https://doi.org/10.1149/2.004207jes

31. M. Šćepanović, Z.D. Dohćević-Mitrović, I. Hinić, M. Grujić-Brojćin, G. Stanisić, Z.V. Popović, Mat. Science Forum. (2005). https://doi.org/10.4028/www.scientific.net/MSF.494.265